A collagen VI–dependent pathogenic mechanism for Hirschsprung's disease

Rodolphe Soret,[1] Mathilde Mennetrey,[1] Karl F. Bergeron,[1] Anne Dariel,[2,3] Michel Neunlist,[3] Franziska Grunder,[4] Christophe Faure,[4] David W. Silversides,[5] and Nicolas Pilon[1] for the Ente-Hirsch study group[6]

[1]Molecular Genetics of Development Laboratory, Department of Biological Sciences and BioMed Research Center, University of Quebec at Montreal (UQAM), Montreal, Quebec, Canada. [2]Department of Pediatric Surgery, Nantes University Hospital, Nantes, France. [3]Inserm, U913, Institut des Maladies de l'Appareil Digestif du Centre Hospitalier Universitaire de Nantes, Nantes, France. [4]Division of Pediatric Gastroenterology, Hepatology and Nutrition, Sainte-Justine University Health Centre, Montreal, Quebec, Canada. [5]Department of Veterinary Biomedicine, Centre de recherche en reproduction animale, Faculty of Veterinary Medicine, University of Montreal, St-Hyacinthe, Quebec, Canada. [6]The Ente-Hirsch study group is detailed in the Supplemental Acknowledgments.

Hirschsprung's disease (HSCR) is a severe congenital anomaly of the enteric nervous system (ENS) characterized by functional intestinal obstruction due to a lack of intrinsic innervation in the distal bowel. Distal innervation deficiency results from incomplete colonization of the bowel by enteric neural crest cells (eNCCs), the ENS precursors. Here, we report the generation of a mouse model for HSCR — named Holstein — that contains an untargeted transgenic insertion upstream of the collagen-6α4 (*Col6a4*) gene. This insertion induces eNCC-specific upregulation of *Col6a4* expression that increases total collagen VI protein levels in the extracellular matrix (ECM) surrounding both the developing and the postnatal ENS. Increased collagen VI levels during development mainly result in slower migration of eNCCs. This appears to be due to the fact that collagen VI is a poor substratum for supporting eNCC migration and can even interfere with the migration-promoting effects of fibronectin. Importantly, for a majority of patients in a HSCR cohort, the myenteric ganglia from the ganglionated region are also specifically surrounded by abundant collagen VI microfibrils, an outcome accentuated by Down syndrome. Collectively, our data thus unveil a clinically relevant pathogenic mechanism for HSCR that involves cell-autonomous changes in ECM composition surrounding eNCCs. Moreover, as *COL6A1* and *COL6A2* are on human Chr.21q, this mechanism is highly relevant to the predisposition of patients with Down syndrome to HSCR.

Introduction

The enteric nervous system (ENS) is located within the gut wall and is mainly composed of multiple interconnected ganglia organized into two main plexuses: the submucosal plexus and the myenteric plexus. The submucosal plexus controls mucosal functions such as electrolyte secretion, paracellular permeability, and epithelial cell proliferation, whereas the key role of the myenteric plexus is to control gastrointestinal motility independently of the central nervous system (1). The vast majority of the neuronal and glial cells that form the ENS is derived from neural crest cells (NCCs), originating from the vagal region of the neural tube. After having reached the foregut, these enteric NCCs (eNCCs) then migrate in a rostral to caudal direction to colonize the midgut and hindgut, between E9.5 and E14.5 in mice (2). In addition to eNCC migration, completion of ENS formation relies on tight control of proliferation, survival, and differentiation of these cells (3, 4). Accordingly, alteration of any of these events can lead to gut motility disorders such as Hirschsprung's disease (HSCR) (5–7).

HSCR is a complex genetic disease that has a global incidence of 1 in 5,000 human births and is characterized by the absence of neural ganglia in the distal gut, from the anus up to a variable length of the intestines. In the majority of cases (80%), the aganglionic zone consists of the rectum and sigmoid colon only (short-segment HSCR), whereas, for most of the remaining cases, it extends toward the proximal end of the colon (long-segment HSCR) (8). Among the numerous genes that have been associated with HSCR (7), the main ones encode members of two key signaling pathways: GDNF/RET and EDN3/EDNRB. Extensive characterization of mouse models bearing loss-of-function alleles of these genes has shown that both of these pathways regulate migration, proliferation, survival, and differentiation of eNCCs (4, 9). However, mutations in these genes or in any other known gene collectively account for less than one-third of HSCR cases (10). In particular, both the 4:1 male sex bias and the strong association with trisomy 21 are intriguing hallmarks of HSCR that currently remain poorly understood, although candidate genes have been suggested (11–15).

The composition of the extracellular matrix (ECM) is another important factor that can influence gut colonization by eNCCs and might thus contribute to HSCR pathogenesis. The ECM is a 3-dimensional acellular structure composed of tissue-specific combinations of a large number of collagens, proteoglycans (e.g., decorin and versican), and glycoproteins (e.g., fibronectin, laminins, and tenascins) (16). In addition to their well-known scaffolding roles (17), ECM proteins can influence cell behavior (i.e., migration, proliferation, survival, and/or differentiation) by inter-

▶ **Related Commentary: p. 4323**

acting with either secreted ligands or transmembrane receptors (18). With respect to eNCCs, such ECM function has been clearly demonstrated by the analysis of NCC-specific *Itgb1*-null mice (19, 20). Indeed, this work revealed that, without β₁ integrin–mediated interactions with ECM proteins, eNCCs fail to fully colonize the hindgut (20), at least in part, because they cannot interact with migration-promoting fibronectin (19). Intriguingly, this latter study also revealed that tenascin-C has an opposite effect on eNCCs (i.e., inhibits migration), whereas another group reported that cell-autonomous production of tenascin-C by eNCCs promotes their migration in chicken embryos (21). In addition to potential species-specific differences (22), these apparent conflicting results might be explained by the fact that different combinations of ECM proteins were used in these ex vivo studies (i.e., tenascin-C with vitronectin and tenascin-C with or without fibronectin, respectively). Although both results suggest that the composition of the ECM is critical for eNCC migration, this has never been assessed in vivo.

Collagens, with 28 different types forming 8 different classes, are the most abundant proteins of the ECM (18). Among these, collagen type VI proteins constitute the highly specific filamentous class. Like every collagen type, collagen VI proteins are first assembled as a trimeric monomer, comprising, in this case, 3 different polypeptide α chains. These trimeric monomers then form antiparallel dimers, which are then laterally associated into tetramers that are secreted in order to form extracellular microfibrils (23). Each collagen VI trimeric monomer is believed to be composed of the α1-α2 pair, to which is added any one of the structurally related α3, α4, α5, or α6 chains (24, 25). These α chains are encoded by individual genes that can be regrouped into "classical" (collagen-6α1–collagen-6α3 [*Col6a1*–*Col6a3*]) and "novel" (*Col6a4*–*Col6a6*) sets (25, 26). *Col6a1* and *Col6a2* form a gene cluster located on Chr.10C1 in mice and on Chr.21q22 in humans, while *Col6a4*, *Col6a5*, and *Col6a6* form a second gene cluster located on Chr.9F1 in mice and on Chr.3q22 in humans. *Col6a3* is located independently on Chr.1D in mice and on Chr.2q37 in humans. Of note, in contrast to its murine ortholog, the human *COL6A4* gene has been converted into 2 nonprocessed pseudogenes *COL6A4P1* and *COL6A4P2*, by a chromosomal break (25, 26).

Expression analyses in embryonic and postnatal gastrointestinal tissues — at both mRNA and protein levels — indicate that, in contrast to the very broad expression of the α1/α2/α3 subunits, expression of the "novel" subunits appears limited to the α4 (embryonic and postnatal) and α5 (postnatal) subunits and in a much more restricted manner (27). During ENS formation, the α4 subunit is notably found distributed within the gut wall, with an internal high to external low radial gradient of expression (27). Moreover, recent transcriptome analyses have revealed that eNCCs express high levels of *Col6a1*, *Col6a2*, and *Col6a3* and low levels of *Col6a4* but do not express *Col6a5* and *Col6a6* (11).

Apart from playing key structural roles (28–32), collagen VI has also been reported to influence cell migration, at least in part, via fibronectin-dependent means (33–35). Regarding NCCs, it has been shown in vitro that their adhesion and initial migration from cultured neural tubes is similarly stimulated by collagen VI and fibronectin (34). On the other hand, in the bowel, it has been shown that epithelial cells are a major site of collagen VI production and that *COL6A1* knockdown in human intestinal epithelial

cells stimulates cell spreading, adhesion, and migration, most likely via increased expression and deposition of fibronectin (33). This work further revealed that collagen VI and fibronectin are closely codistributed around cultured intestinal epithelial cells and that lack of collagen VI affects the microfibrillar organization of fibronectin, an outcome also previously reported by others in cultured fibroblasts (35) and which is in accordance with the fact that collagen VI can bind fibronectin (35–37). To the best of our knowledge, neither the specific role of collagen VI on eNCC migration nor the general consequence of overexpressing collagen VI has been reported so far.

In this work, we report the generation and characterization of what we believe to be a novel insertional mutant mouse line, in which eNCCs specifically overexpress *Col6a4*. We show that increased cell-autonomous deposition of collagen VI around mutant eNCCs inhibits their migration, most likely by interfering with fibronectin, and thereby leads to an aganglionic megacolon phenotype reminiscent of short-segment HSCR. Analysis of the ganglionated regions of patients with short-segment HSCR with and without Down syndrome strongly suggests that this pathogenic mechanism that we believe to be novel is common and, combined with the fact that *COL6A1* and *COL6A2* are located on Chr.21q, may provide a mechanistic explanation for the strong association between trisomy 21 and HSCR.

Results

Description of the Holstein mouse line. The Holstein mouse line was generated via an insertional mutagenesis screen for genes important in NCCs, which also yielded the recently described TashT line (11). The screening strategy was based on the random insertion of a tyrosinase (*Tyr*) minigene in the FVB/N genetic background (38). As *Tyr* can rescue melanin production by the NCC-derived melanocytes of this albino strain, animals with abnormal NCC development were identified by the simple presence of nonuniform pigmentation patterns (11). Named after the well-known dairy cow, heterozygous Holstein (*Hol^{Tg/+}*) mice are easily recognizable due to the presence of large pigmented areas in their otherwise white fur (Figure 1A). Homozygous Holstein (*Hol^{Tg/Tg}*) animals can be obtained from heterozygous intercrosses at the expected Mendelian frequency and are also easily recognizable owing to their extensive depigmentation, with only a single pigmented patch on their back. Importantly, no *Hol^{Tg/Tg}* animals lived beyond weaning age, and they all exhibited symptoms typically observed in mice suffering from functional intestinal obstruction, such as growth delay, ruffled fur, hunched posture, and abdominal distention (Figure 1, A–C).

One hundred percent of Hol^{Tg/Tg} animals die from aganglionic megacolon. In accordance with the age of death and the symptoms mentioned above, gross observations of internal organs of *Hol^{Tg/Tg}* animals (either found dead or sacrificed; >50 cases observed) pointed to marked dilatation of the proximal and mid-colon (megacolon) together with narrowing of the distal colon as the only obvious defect (Figure 1C). To confirm aganglionosis as the cause of megacolon, we then examined the myenteric plexuses of P20 animals obtained from *Hol^{Tg/+}* intercrosses via staining for acetylcholinesterase (AchE) activity in gut muscle strips (Figure 1, D–F). This analysis revealed that, while no obvious differ-
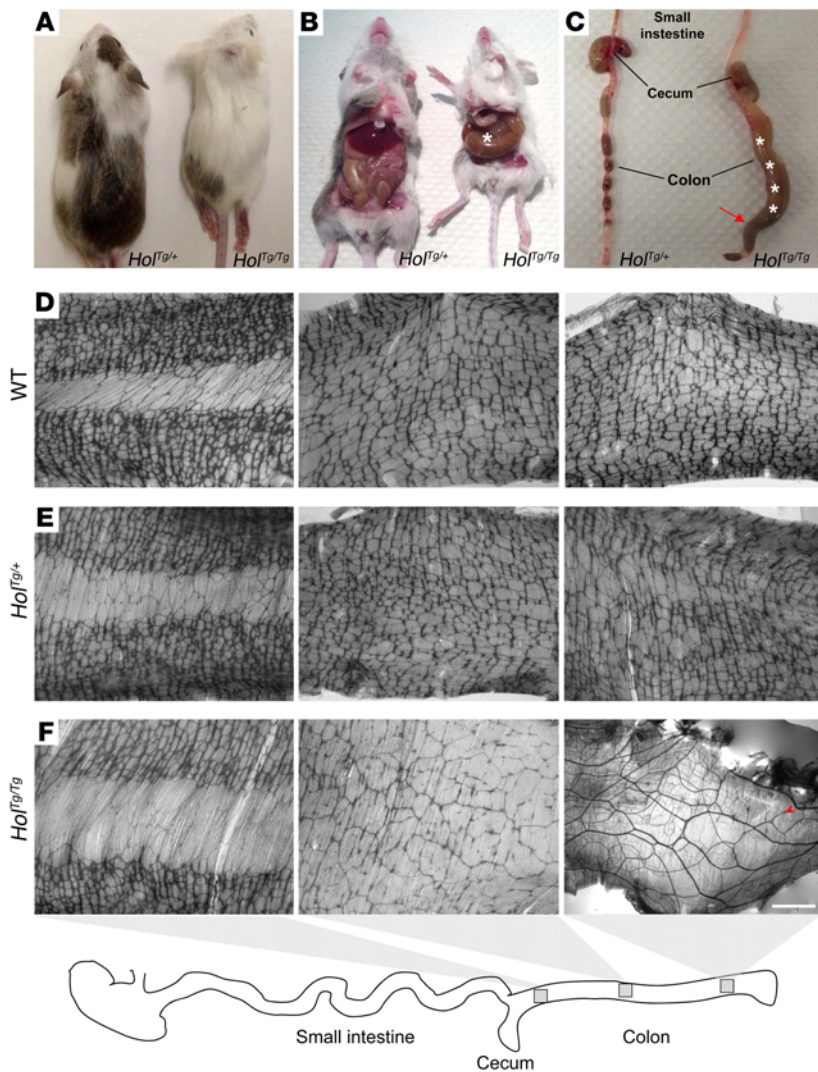
Figure 1. The Holstein mouse line is a model for aganglionic megacolon. (**A**) Comparison between heterozygous ($Hol^{Tg/+}$) and homozygous ($Hol^{Tg/Tg}$) Holstein animals from a F2 litter at P20, showing allele dosage-dependent depigmentation. (**B**) $Hol^{Tg/Tg}$ mutants are smaller than their littermates and exhibit symptoms of aganglionic megacolon (asterisk). (**C**) These animals die due to blockage in the distal colon (arrow) and massive accumulation of fecal material (asterisks). (**D**–**F**) Labeling of the myenteric plexus in the colons of (**D**) wild-type, (**E**) $Hol^{Tg/+}$, and (**F**) $Hol^{Tg/Tg}$ P20 mice via staining of AchE activity. In comparison to wild-type mice ($n = 8$) and $Hol^{Tg/+}$ controls ($n = 7$), the ENS network of $Hol^{Tg/Tg}$ animals ($n = 12$) is very slightly less dense in the proximal colon (left), is scarce and less interconnected in the mid-colon (middle), and is markedly absent in the distal colon (right), in which hypertrophic extrinsic nerve fibers typical of aganglionic megacolon as well as very rare isolated nerve cell bodies (red arrowhead) are seen. Scale bar: 1,000 μm.

ences are observed in the proximal colon, myenteric ganglia are completely absent in the distal colons of $Hol^{Tg/Tg}$ animals. Rather, this region contains a high number of large extrinsic nerve fibers devoid of ganglia as well as the occasional presence of isolated neurons. Moreover, this aganglionic zone is preceded by a transition zone in the mid-colon characterized by a marked decrease of ENS density. Both the presence of large extrinsic nerve fibers and the presence of a transition zone are hallmarks of aganglionic megacolon (39). Quantification of the ENS length in the colons of these animals showed that males (ganglionated on average over 72.5% of colon length) and females (ganglionated on average over 75.9% of colon length) were similarly affected (Supplemental Figure 1; supplemental material available online with this article; doi:10.1172/JCI83178DS1), both displaying an extent of ganglionosis below the minimal threshold (~80%) that we have recently described for mice of the FVB/N background (11). To determine at which stage the $Hol^{Tg/Tg}$ defect appears during ENS formation, the extent of eNCC colonization was analyzed via whole-mount immunofluorescence staining with an antibody directed against βIII-tubulin. This analysis revealed that, starting at E11.5 and persisting until birth, gut colonization by eNCCs was significantly delayed in $Hol^{Tg/Tg}$ tissues (Figure 2).

The Holstein transgenic insertion leads to specific Col6a4 overexpression in eNCCs. To identify the genetic cause of the Holstein phenotype, we first localized the site of transgene insertion via high-throughput sequencing of a $Hol^{Tg/Tg}$ mouse genome. Following mapping of paired sequencing reads, an analysis of the *Tyr* locus focused on exons and regulatory sequences allowed us to identify apparent translocation events that were in fact representative of the transition between the *Tyr* transgene and the insertion site. Via PCR amplification and Sanger sequencing of such events, we precisely localized the insertion site on chromosome 9 between the *Col6a4* (at ~11.3 kb) and glycerate kinase (*Glyctk*; at ~44.6 kb) genes (Figure 3A). From the mapping data, we also estimated the number of transgene copies and, by extension, the size of the transgenic insertion to be approximately 11 transgene copies and approximately 74 kb, respectively. We further noted that this insertion is accompanied by a 153-bp deletion, which allowed us to design a robust PCR genotyping assay (Figure 3, A and B).

We then tested the effect of the transgenic insertion on the expression of surrounding genes via semiquantitative RT-PCR on whole-embryonic intestines as well as on eNCCs recovered by FACS. It is noteworthy that the later was made possible by backcrossing the Holstein allele onto a Gata4p[5 kb]-RFP (G4-RFP)
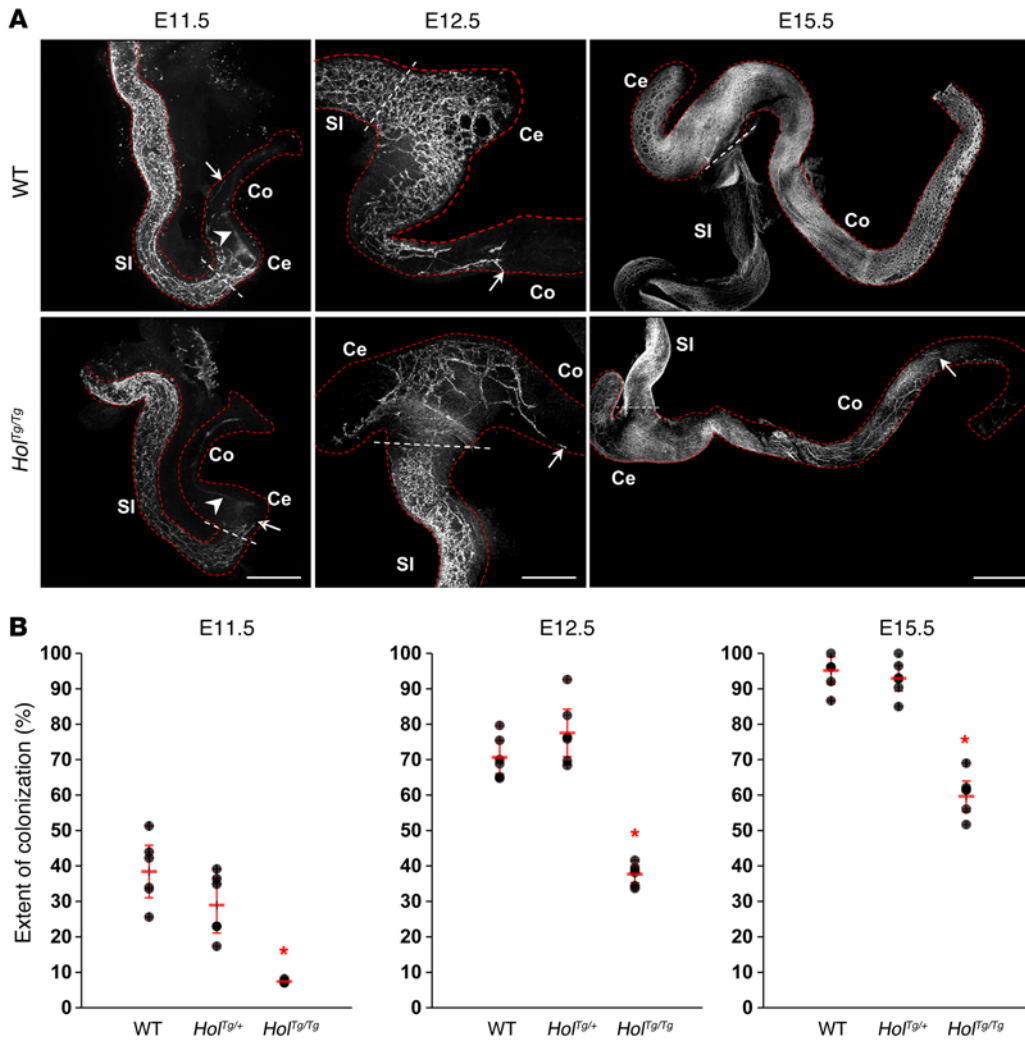
Figure 2. Defective ENS formation in *Hol^{Tg/Tg}* embryos is detected from E11.5 onward. (**A**) Analysis of eNCC colonization in embryonic intestine at E11.5 (left; scale bar: 430 μm), E12.5 (middle; scale bar: 200 μm), and E15.5 (right; scale bar: 700 μm), using an anti–βIII-tubulin antibody. Arrows point to the most distal neuronal-fated eNCC of vagal origin, while arrowheads point to nonspecific staining of the meconium. SI, small intestine; Ce, cecum; Co, colon. (**B**) Quantification of the extent of eNCC colonization (at E11.5, E12.5, and E15.5) as measured from the base of cecum (white dashed lines in **A**) to the most distally located neuronal-fated eNCC of vagal origin. In comparison to that in wild-type tissues, the extent of bowel colonization by *Hol^{Tg/Tg}* eNCCs is significantly decreased (data are presented as mean ± SEM; for each stage, $n = 6$ intestines per genotype; $*P < 0.01$; 1-way ANOVA).

background, which allows labeling of migratory NCCs with the red fluorescent protein DsRed2 (40). For these expression analyses, we chose to use E12.5 intestines, as they are easy to dissect and are clearly affected by the Holstein colonization defect. Although *Col6a4* expression appeared unchanged in whole-gut tissues (Figure 3C), a strong and allele dosage–dependent overexpression was found in Holstein eNCCs compared with that in wild-type eNCCs (Figure 3D). This effect was found to be specific to *Col6a4*, as both *Col6a5* and *Col6a6* remained unexpressed, while expression levels of *Glyctk* and *Wdr82* were found to be identical in *Hol^{Tg/Tg}* and control G4-RFP eNCCs (data not shown). To validate our RT-PCR data and determine whether other genes might be affected by the transgenic insertion, we profiled the rRNA-depleted transcriptome via RNA sequencing (RNAseq) of FACS-recovered E12.5 eNCCs (*Hol^{Tg/Tg}* G4-RFP vs. control G4-RFP). This analysis indicated that *Col6a4* is by far the most dramatically affected gene in terms of both the fold change and the statistical significance (Figure 3E and Supplemental Data Set 1). Neither genes known to be associated with HSCR/ENS development nor other collagen genes were found to be modulated beyond the typical 2-fold cutoff (Supplemental Data Set 1).

To assess whether the observed *Col6a4* overexpression is correlated with increased collagen VI deposition in the ECM sur-

rounding eNCCs, we then carried out immunofluorescence analyses using a polyclonal collagen VI antibody. As expected, analyses of E12.5 intestines revealed an increase in collagen VI protein levels in *Hol^{Tg/Tg}* tissues and, importantly, specifically in the plane of migratory eNCCs (Figure 4 and Supplemental Figure 2). Similar observations were made at other stages of development (E11.5 and E15.5; Supplemental Figures 3 and 4), and, in each case, high levels of collagen VI were found in a mutually exclusive manner with neuronal-fated eNCCs (Supplemental Figure 2). Such an increase was not detected at, or beyond, the migration front of *Hol^{Tg/Tg}* eNCCs (Figure 4A). It is also noteworthy that strong collagen VI staining was consistently observed postnatally, not only at the periphery of myenteric ganglia but also within myenteric ganglia (in a mutually exclusive manner with enteric neurons) of *Hol^{Tg/Tg}* P21 animals (Supplemental Figure 5). This implies that collagen VI produced during development can persist postnatally and/or that collagen VI is continuously secreted by intraganglionic cells.

Intriguingly, our expression analyses revealed a striking difference between the increase in collagen VI protein levels in *Hol^{Tg/Tg}* tissues (~3-fold increase) and the increase in *Col6a4* mRNA levels in *Hol^{Tg/Tg}* eNCCs (~250-fold increase). However, such an outcome is not surprising, given the fact that production of mature collagen VI microfilaments depends on the α1-α2 chain pair (24,
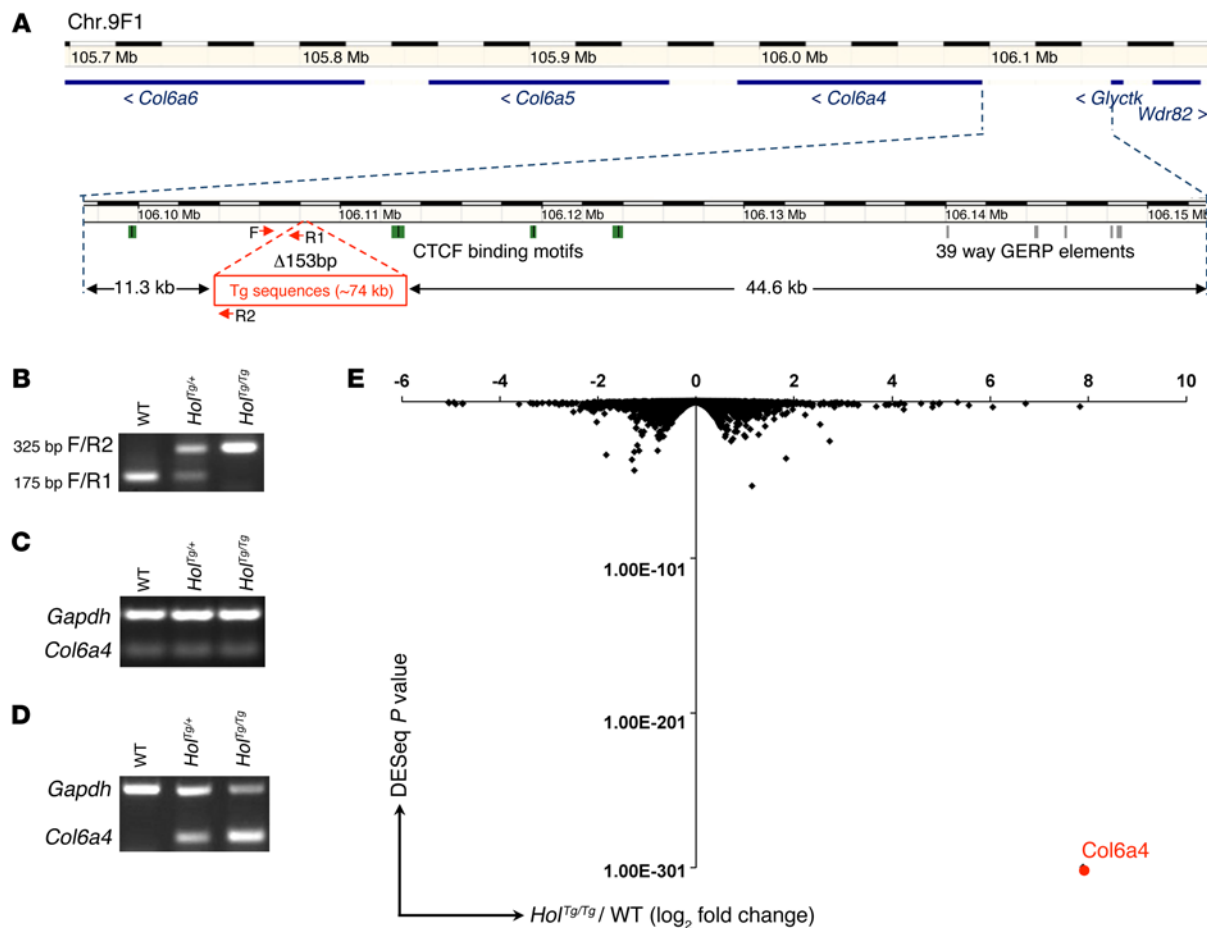
Figure 3. The Holstein transgenic insertion upregulates *Col6a4* expression in eNCCs. (**A**) Schematic representation of the Holstein transgene insertion site based on whole-genome sequencing data and adapted from the Ensembl website (www.ensembl.org). Transgenic sequences are inserted in a 153-bp deletion (Δ 153 bp) between the *Col6a4* and *Glyctk* genes on mouse Chr.9F1, which is syntenic to human Chr.3q22. Analysis of this region with the regulation track of Ensembl revealed the presence of multiple CTCF-binding motifs (green boxes) in the vicinity of the transgene insertion site, whereas the Comparative Genomics track (Genomic Evolutionary Rate Profiling [GERD] for 39 eutherian mammals; gray boxes) revealed that highly conserved noncoding sequences are not found close to the insertion site. (**B**) Example of PCR-based genotyping of Holstein animals using the oligos depicted in **A** (see Supplemental Table 2 for primers F/R1 and F/R2). (**C** and **D**) Analysis of *Col6a4* transcript levels in E12.5 embryos via semiquantitative RT-PCR. (**C**) In contrast to that in whole intestines, a (**D**) robust allele dosage-dependent increase in *Col6a4* gene expression is observed in FACS-recovered eNCCs. (**E**) Volcano plot of RNAseq-based comparative analysis of global gene expression between *Hol*[Tg/Tg] and wild-type eNCCs recovered by FACS from E12.5 intestines (*n* = 3 groups of 5–6 intestines per genotype). The log2 fold-change is on the *x* axis, while the DESeq *P* value is on the *y* axis.

25). Indeed, as both *Col6a1* and *Col6a2* were not overexpressed in *Hol*[Tg/Tg] eNCCs (Supplemental Data Set 1), the amount of α1-α2 chain pairs was thus most likely the limiting factor for the relatively modest overproduction of α1-α2-α4 trimeric monomers that we observed. Regardless of the exact order of magnitude involved, our expression data suggest a pivotal role for eNCC-specific *Col6a4* overexpression in the developmental origin of the *Hol*[Tg/Tg] megacolon phenotype.

Colonic aganglionosis in Hol[Tg/Tg] *animals is caused by a cell-autonomous defect in eNCC migration.* To further characterize the colonization defect of *Hol*[Tg/Tg] eNCCs, we first sought to confirm its cell-autonomous nature via heterotopic grafts of E12.5 embryonic guts. To this end, we again took advantage of the presence of the Holstein allele on the G4-RFP background and compared the ability of eNCCs from mutant and control midgut segments to colonize control aneural hindgut segments. In contrast to control G4-RFP eNCCs, *Hol*[Tg/Tg] G4-RFP eNCCs were poorly able to colo-

nize hindgut tissues in this experimental setting (~3-fold less efficient on average), clearly demonstrating that non-eNCCs are not responsible for the *Hol*[Tg/Tg] phenotype (Figure 5, A and B). Then, in an effort to identify which cellular process might be deregulated in *Hol*[Tg/Tg] eNCCs, we analyzed the migration speed and directionality of leading eNCCs (i.e., at the tips of eNCC chains) in cultured E12.5 and E13.5 whole intestines using time-lapse imaging (Figure 5C and Supplemental Videos 1 and 2). This analysis revealed that, at each stage examined, the mean migration speed of *Hol*[Tg/Tg] G4-RFP eNCCs was about half of that of control G4-RFP eNCCs (Figure 5D), while directionality appeared unaffected (Supplemental Figure 6).

To test whether other processes might contribute to the *Hol*[Tg/Tg] phenotype, we subsequently evaluated neuronal and glial differentiation as well as eNCC proliferation and cell death. Comparative analysis of cell differentiation in *Hol*[Tg/Tg] and wild-type embryonic guts revealed that, while the number of neurons appeared unaf-
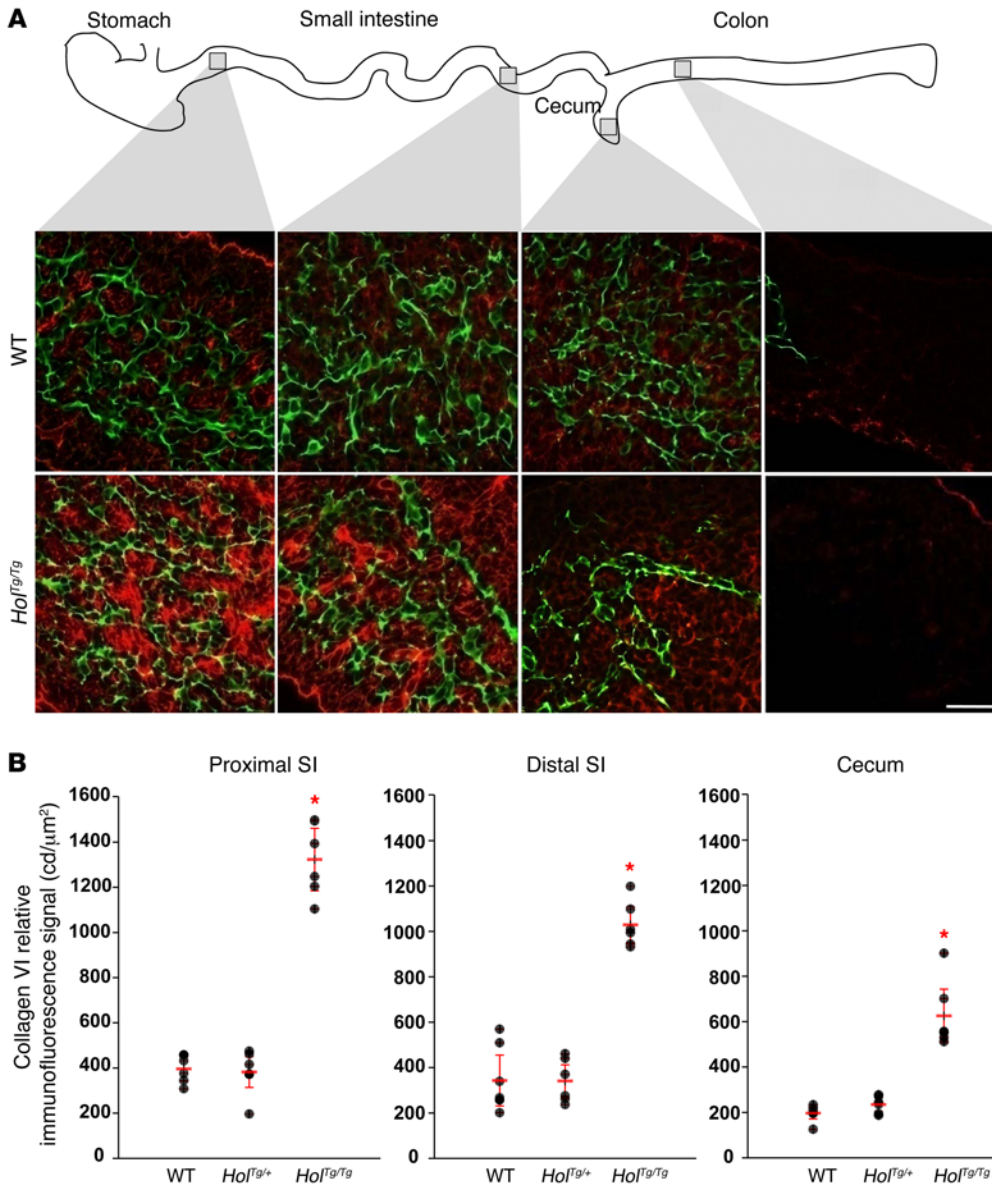
Figure 4. Collagen VI protein levels are increased in E12.5 *Hol^{Tg/Tg}* intestines. (**A**) Single confocal sections in the plane of the developing myenteric plexus in wild-type and *Hol^{Tg/Tg}* E12.5 intestines doubly labeled with anti–collagen VI (red) and anti–βIII-tubulin (green) antibodies. Scale bar: 20 μm. (**B**) Quantification of collagen VI immunofluorescence signals in candelas (cd) per μm², showing that collagen VI protein levels are significantly increased in *Hol^{Tg/Tg}* embryonic intestines colonized by neuronal-fated eNCCs (data are presented as mean ± SEM; $n = 6$ intestines per genotype; $*P < 0.01$; 1-way ANOVA).

fected at both E12.5 (Supplemental Figure 7) and E15.5, a reduced glia/progenitor cell ratio was observed in E15.5 *Hol^{Tg/Tg}* tissues (Supplemental Figure 8). However, regardless of the mechanism involved, this argues against the idea that premature differentiation underlies the Holstein migration defect. Furthermore, neither proliferation nor TUNEL⁺ cell death was found to be affected in *Hol^{Tg/Tg}* eNCCs (Supplemental Figure 9).

Collagen VI interferes with the migration-promoting effects of fibronectin ex vivo. To begin understanding how an excess of collagen VI can slow down the migration speed of eNCCs, we first evaluated the ability of this ECM component to promote migration in comparison to other ECM proteins. To this end, we cultured G4-RFP midgut slices on different coatings over 48 hours in the presence of glial cell line–derived neurotrophic factor (GDNF), a well-known and potent chemoattractant for eNCCs (41, 42). Of the 4 tested coatings (fibronectin, gelatin, collagen I, and collagen VI), fibronectin was found to be the most effective in promoting migration of fluorescent eNCCs out of the explants, whereas collagen I and VI were

found to be equally inefficient (Figure 6, A and B). Interestingly, we then observed that, when used in conjunction with fixed amounts of fibronectin, increasing amounts of collagen VI lead to a dosage-dependent decline in the net distance traveled by fluorescent eNCCs in response to GDNF (Figure 6C). To determine whether cell-autonomous secretion of collagen VI by eNCCs is enough for reproducing this outcome, we compared the net distance traveled by *Hol^{Tg/Tg}* and wild-type eNCCs using the same approach. Importantly, such GDNF-stimulated and fibronectin-promoted migration of eNCCs from midgut explants was found to be significantly less efficient using *Hol^{Tg/Tg}* tissues (Figure 6D). Altogether, our ex vivo analyses allow us to propose a pathogenic mechanism whereby greater cell-autonomous secretion of collagen VI by *Hol^{Tg/Tg}* eNCCs interferes with the migration-permissive ECM of the developing gut wall, which is known to be especially enriched in fibronectin (refs. 19, 21, 43, and Supplemental Figure 10).

Myenteric ganglia of patients with HSCR are surrounded by abundant collagen VI microfibrils. Finally, to determine whether
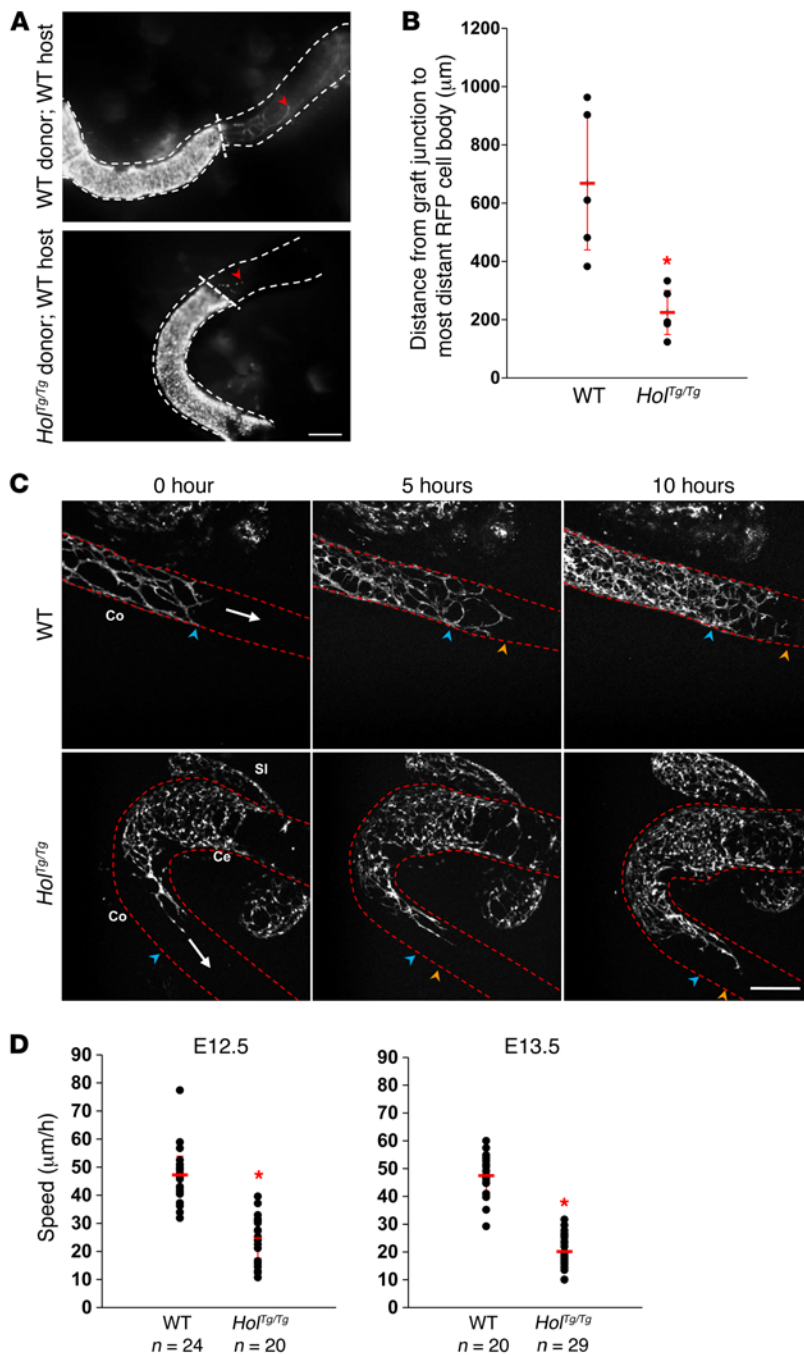
Figure 5. Cell-autonomous defect in *Hol^{Tg/Tg}* eNCC migration. (**A**) Representative images of heterotopic E12.5 midgut-hindgut grafts after 24 hours of culture, showing that colonization of WT host tissues (aneural hindgut segments) by RFP-labeled eNCCs is much less efficient with mutant (*Hol^{Tg/Tg}* G4-RFP) than with control (WT G4-RFP) midgut segments as donor tissues. Red arrowheads point to the location of the migration front at the end of the culture period. Scale bar: 150 μm. (**B**) Quantitative analysis of the extent of hindgut colonization by eNCCs coming from midgut tissues (data are presented as mean ± SEM; n = 5 grafts per combination; *$P < 0.001$; Student's t test). (**C**) Representative images from 10-hour-long time-lapse recordings of eNCC movement at the migration front in WT and *Hol^{Tg/Tg}* E13.5 intestines. The white arrows indicate the direction of colonization, whereas blue and orange arrowheads point to the location of the migration front at the start and end of recordings, respectively. Scale bar: 100 μm. (**D**) Quantification of the speed of individual cells at the tip of the migration front shows that *Hol^{Tg/Tg}* eNCCs are significantly slower than WT eNCCs at both the E12.5 and E13.5 stages (data are presented as mean ± SEM; n represents the total number of cells from at least 3 intestines; *$P < 0.01$; Student's t test).

ganglia) should be specifically detected in HSCR tissues, as observed in *Hol^{Tg/Tg}* postnatal bowels (Supplemental Figure 5). Accordingly, our immunofluorescence analyses showed that collagen VI levels appeared generally increased at the periphery of myenteric ganglia from patients with HSCR (Figure 7A and Supplemental Figure 11). Phenotype-stratified quantitative analyses revealed that, in comparison with those in controls, periganglionic collagen VI levels were on average doubled in patients with HSCR and tripled in patients with HSCR and Down syndrome (Figure 7B and Supplemental Table 1). Importantly, only a small overlap was noted between the highest values in the control group and the lowest values in the HSCR group. Assuming a normal distribution for each group, the extent of such overlap was estimated to be limited to 22%. Interestingly, similar intergroup differences were also observed for intraganglionic collagen VI levels (Supplemental Table 1), although no strong correlation between intraganglionic and periganglionic collagen VI could be consistently detected (r = 0.82 for controls; r = 0.63 for patients with HSCR; r = 0.17 for patients with HSCR and Down syndrome). Moreover, no correlation between age and collagen VI levels emerged from these analyses. In conclusion, our data strongly suggest that to our knowledge we have unveiled a new pathogenic mechanism for HSCR that appears to be common.

Discussion

In this study, we report the generation and characterization of a mouse model for short-segment HSCR called Holstein. The distinctive feature of this model is the eNCC-specific overexpression of *Col6a4*, which encodes a major component of the ECM. Detailed analysis of *Hol^{Tg/Tg}* eNCCs during gut colonization

increased cell-autonomous secretion of collagen VI by enteric neural progenitors might represent a novel clinically relevant pathogenic mechanism for HSCR, we analyzed collagen VI protein distribution in cross sections of muscle strips (i.e., muscle layers and myenteric plexus) prepared from ganglionated colonic tissues of human patients with HSCR and controls. Our HSCR cohort consisted of 12 children diagnosed with isolated short-segment HSCR and 4 children diagnosed with combined HSCR and Down syndrome, whereas our control cohort consisted of 8 children diagnosed with an isolated gastrointestinal malformation not primarily involving the ENS (Supplemental Table 1). We reasoned that, if the proposed pathogenic mechanism was true, then abnormal deposition of collagen VI (both around and within myenteric
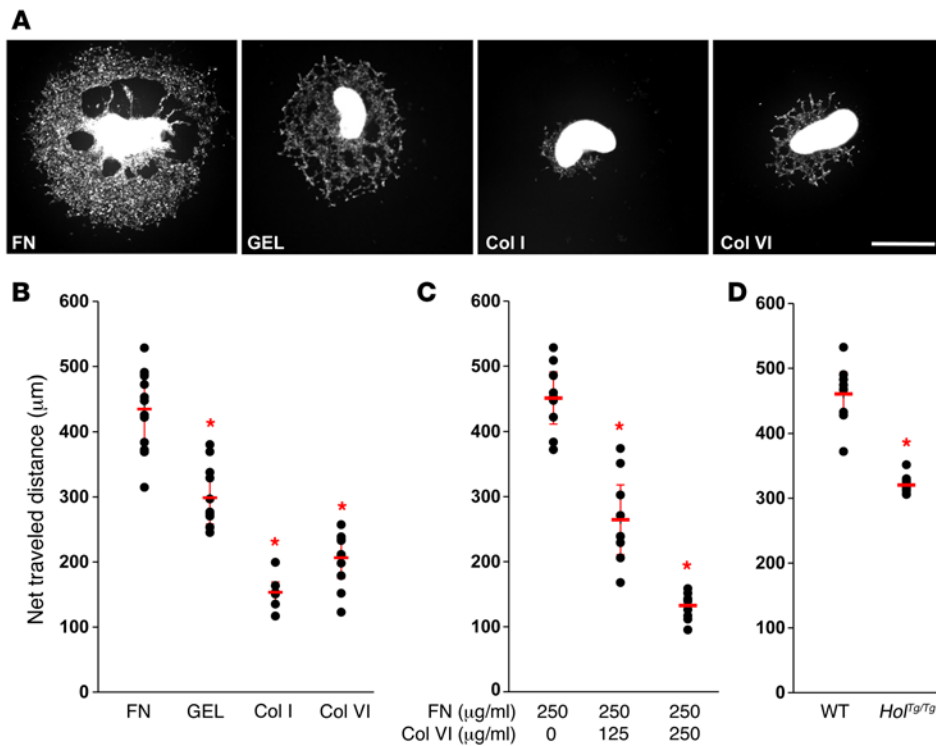
Figure 6. Collagen VI negatively impacts GDNF-stimulated eNCC migration ex vivo. (**A**) Representative low-magnification views of E12.5 G4-RFP midgut explants cultured on the indicated coatings for 48 hours in GDNF-supplemented medium. FN, fibronectin; GEL, gelatin; Col I, collagen I; Col VI, collagen VI. Scale bar: 500 μm. (**B**–**D**) Quantitative analysis of the net distance traveled, on average, by RFP-labeled eNCCs farthest from the edges of the explant (n = 8 cells per explants; 1 cell per quadrant) at the end of the 48-hour culture (data are presented as mean ± SEM; $n \geq 10$ explants per condition from 4 independent experiments; *$P < 0.01$; 1-way ANOVA in **B** and **C**; Student's t test in **D**). (**B**) Note that both collagens are inefficient in promoting eNCC migration and (**C**) that increased dosage of collagen VI inhibits the migration-promoting effects of fibronectin. (**D**) In addition, note that, in comparison to WT G4-RFP explants, eNCC migration on fibronectin is significantly less efficient when using $Hol^{Tg/Tg}$ G4-RFP explants.

allowed us to identify a pathogenic mechanism for HSCR involving cell-autonomous modulation of the eNCC microenvironment. Analysis of patient tissues indicated that this mechanism appears to be common and is even more pronounced in patients who also have Down syndrome. Therefore, combined with the fact that the genes encoding the key subunits for collagen VI assembly are located on human Chr.21q, this allows us to propose a possible molecular explanation for the strong association between Down syndrome and HSCR.

Is the missing heritability of HSCR hidden in the regulatory genome? RET was the first gene for which mutations were shown to be associated with HSCR (44, 45), and, more than 20 years later, this remains the most frequently observed association in large cohorts (46). However, HSCR is a complex genetic disease for which only a small subset of cases can be explained by mutations in *RET* or other known genes (10). As such, the hunt for HSCR genes remains an active field of research (10, 46–48). Very interestingly, our forward genetic screen — aimed at identifying genes with key roles in NCCs — has yielded 3 mouse lines with aganglionic megacolon: TashT (11), Holstein (as described in this article), and Spot (data not shown). Phenotypically, homozygous mutant TashT mice display a variably penetrant megacolon, with a male-versus-female bias, reminiscent of the presentation of HSCR within the human population (8). In contrast, homozygous mutant Holstein mice show invariant penetration of the megacolon phenotype without a sex bias. Most importantly, all 3 lines share the fact that aganglionic megacolon results from insertional mutagenesis-induced overexpression of genes within eNCCs — genes that have not previously been associated with HSCR and/or ENS development. For the TashT line, we have shown that megacolon is due to perturbation of ultra-long-range interactions between silencer elements and at least the *Fam162b* gene (11). What causes *Col6a4*

overexpression in the Holstein line is currently unknown. In contrast to TashT, flanking sequences in the vicinity of the Holstein transgene insertion site are devoid of highly conserved regions suggestive of a regulatory function. In addition, we tested the possibility that the 153-bp deletion at the Holstein transgene insertion site might contain a poorly conserved repressor element, but these sequences did not exhibit such activity when used in a luciferase reporter construct driven by the thymidine kinase minimal promoter (Supplemental Figure 12). Another possibility might be that the transgenic sequences located 11.3 kb upstream might by themselves activate *Col6a4* expression. However, the fact that the combined expression of both endogenous and transgenic tyrosinase was very low in eNCCs strongly argues against this hypothesis (Supplemental Data Set 1). On the other hand, the observation that multiple CTCF-binding motifs are located around the transgene insertion site strongly suggests that *Col6a4* on the centromeric side is normally insulated from the genes located on the telomeric side (Figure 3A). Indeed, such motifs are known to be critical for maintaining the boundaries between topologically associating domains (TADs), which are themselves required for maintaining proper enhancer-promoter interactions (49–51). Importantly, it has also been recently reported that structural variations that affect TAD boundaries can perturb appropriate gene expression and thereby cause human diseases (52). We thus suggest that the Holstein transgenic insertion may perturb the normal tridimensional chromatin structure of the region, consequently preventing a repressive interaction and/or generating an activating interaction between distal regulatory elements and *Col6a4*. In strong support of this possibility, the vast majority of the genes located between *Glyctk* and *Rrp9* (spanning ~335 kb on the telomeric side of the transgene insertion site) are expressed in eNCCs, including *Wdr82*, *Rpl29*, and *Pcbp4*, which display very robust expression
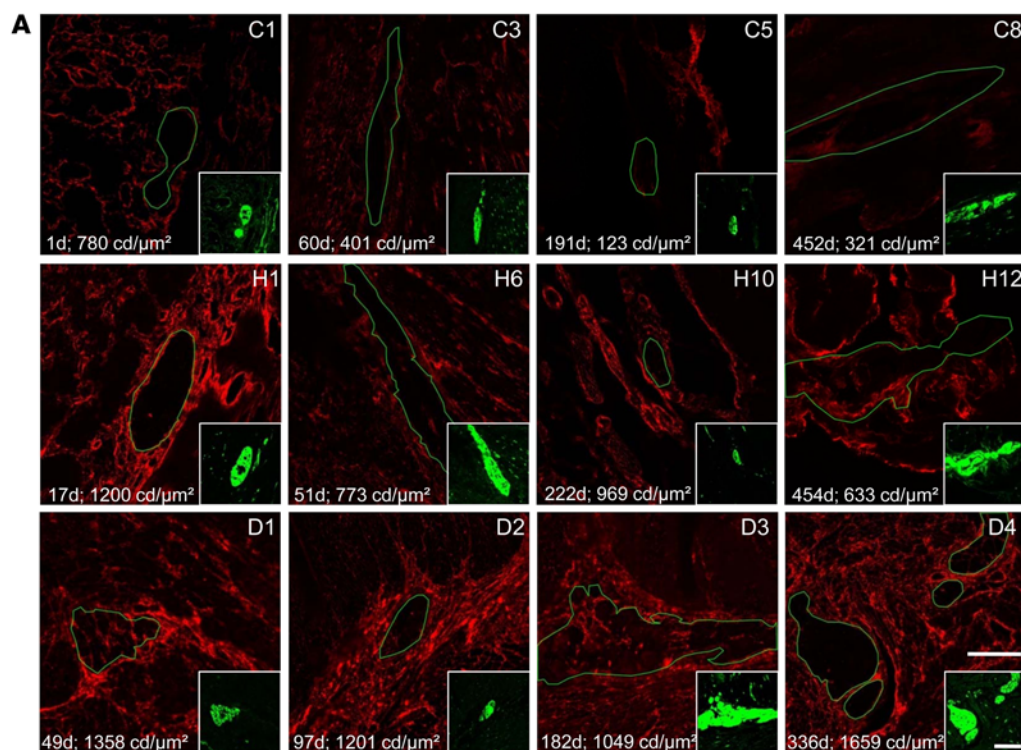
Figure 7. Myenteric ganglia of human patients with HSCR are surrounded by abundant collagen VI microfibrils. (A) Representative single confocal sections of transverse cuts of human colonic muscles double labeled with antibodies against βIII-tubulin (green; in the insets) and collagen VI (red). Myenteric ganglia are delineated by green lines. The identification number for controls (C), patients with HSCR (H), and patients with Down syndrome and HSCR (D) is indicated in the top right corner of each image. Age at the time of tissue collection (indicated in days) as well as average levels of periganglionic collagen VI ($n \geq 5$ ganglia per child's sample; expressed in candelas per μm^2) are indicated in the bottom left corner of each image. Scale bar: 50 μm (insets, 75 μm). **(B)** Quantification data of average periganglionic collagen VI levels for all tested human samples (data are presented as mean ± SEM; *$P < 0.001$ in comparison to controls; #$P < 0.05$ in comparison to patients with HSCR; 1-way ANOVA).
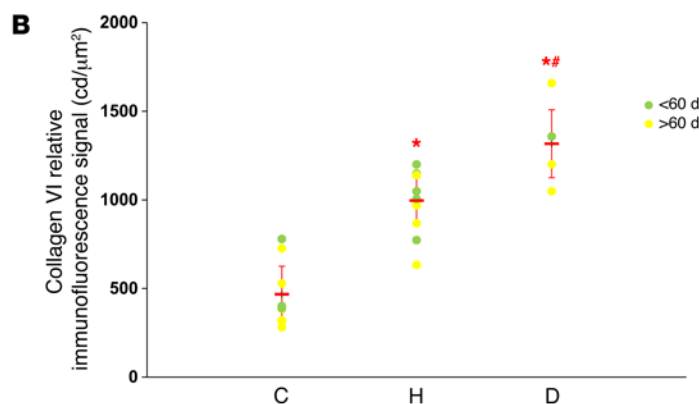
(Supplemental Data Set 1). Regardless of the exact mechanism involved in the case of Holstein or any of our other lines, it is clear that obtaining similar results using more common forward genetic screen methods (e.g., ENU mutagenesis) would have been virtually impossible. On a technical level, our approach offers important advantages in that the mutagenic sequences can be used as a screening tool per se and can also facilitate localization of the insertional mutation via whole-genome sequencing. In addition, our approach offers the key conceptual advantage that it allows for small-scale genomic rearrangements — such as insertions, duplications, and deletions — that are seen much more frequently (>100 times) than single nucleotide polymorphisms in the human genome (53, 54). Above all, our forward genetic screen results strongly support the idea that a large part of the missing heritability of HSCR is hidden in noncoding sequences.

A pathogenic mechanism for HSCR involving cell-autonomous modulation of the ECM by eNCCs. Although the constantly changing composition of the ECM during ENS formation has long been

suspected to play an important role in the colonization of the gastrointestinal tract by eNCCs (43, 55), confirmation of its participatory role has been lacking. This is believed to be due, at least in part, to the fact that genetic deletion of specific ECM proteins is often incompatible with embryonic development (56). Circumventing this problem would require conditional approaches, but these, in turn, require proper knowledge of the cell type(s) expressing the ECM protein to target in a tissue. Current data indicate that different cell types may contribute to the synthesis of the ECM found in the gut wall, including eNCCs themselves (21, 33). In this regard, our previous transcriptome data for eNCCs clearly showed that these cells are actively involved in the formation and modulation of the ECM during development (11). Indeed, as again seen here (Supplemental Data Set 1), eNCCs robustly express a high number of genes encoding ECM proteins, including fibronectin, tenascins, fibulins, and a wide variety of laminin and collagen types. Considering that other intestinal cell types also secrete ECM proteins, this emphasizes the fact that the ECM of the gut wall is composed

of a complex mixture of proteins in which the source and relative abundance of each protein is unknown. Such complexity would be virtually impossible to recreate in a petri dish. On the other hand, in vitro studies are well suited for studying the relative contribution of specific ECM proteins. For example, fibronectin has been widely studied in vitro and is known to promote cell adhesion and migration of several cell types, including eNCCs (19, 21). In marked contrast, collagen VI has been much less studied in this context and consequently little is known regarding its role in cell adhesion and migration. Intriguingly, collagen VI has been reported to promote cell adhesion and migration of trunk NCCs emigrating from quail neural tube explants (34), whereas the converse was reported for cultured human intestinal epithelial cells (33). Apart from the fact that different experimental approaches as well as different animal models were used in these studies, these opposing effects might simply be explained by the fact that collagen VI has different roles depending on the cell type. Our results indicate that the response of vagal-derived eNCCs to collagen VI was similar to that of intestinal epithelial cells rather than to that of NCCs emigrating from the trunk region (Figure 6, A and B). Such striking differences between these two NCC populations is, however, not surprising, given the known differences in their respective molecular signatures (57). Very interestingly, the response of vagal-derived eNCCs to collagen VI appears similar to that of intestinal epithelial cells not only in terms of the output of migration observed but also in terms of the mechanism involved. Indeed, as Groulx et al. (33) observed for intestinal epithelial cells, we found that collagen VI interferes with the promoting effects of fibronectin on eNCC migration. This effect most likely explains why increased secretion of collagen VI by $Hol^{Tg/Tg}$ eNCCs hinders bowel colonization, although the precise mechanism by which this occurs is currently unknown. Based on the fact that collagen VI and fibronectin are known to directly interact with each other (35–37), two possibilities can be considered. On one hand, as previously shown with cultured fibroblasts and intestinal epithelial cells (33, 35), increased collagen VI deposition might negatively affect fibronectin deposition and/or assembly around $Hol^{Tg/Tg}$ eNCCs. However, our immunofluorescence results argue against this possibility, as they failed to reveal overt changes in fibronectin levels and/or organization in $Hol^{Tg/Tg}$ embryonic guts (Supplemental Figure 10). Alternatively, increased levels of collagen VI (migration inhibiting) might compete with fibronectin (migration promoting) for binding of β_1 integrin at the surface of $Hol^{Tg/Tg}$ eNCCs. This possibility is supported by the facts that both collagen VI and fibronectin are bound by β_1 integrin (33) and that β_1 integrin–mediated interactions with the ECM are critically required for eNCC migration (19).

Association between Down syndrome and HSCR may be explained by trisomy 21–induced overexpression of COL6A1 and COL6A2. With an incidence of approximately 1 in 800 live births, Down syndrome (trisomy 21) is one of the most frequently encountered birth defects within the human population. Analysis of subjects with rare segmental trisomies established that Down syndrome results from the 50% increased dosage of a subset of genes that are located within the distal region of the long arm of chromosome 21 (13, 58). Down syndrome has a complex and variable phenotypic presentation, characterized by mental retardation together with different developmental anomalies, depending on

the specific trisomic fragment involved and including HSCR in approximately 1% of cases (7, 13). Present in up to 10% of HSCR cases, trisomy 21 is the most frequently encountered syndromic genetic disorder associated with HSCR (8). All of these observations imply that Down syndrome is not sufficient by itself for developing HSCR and that other factors are required. One of these factors appears to be a hypomorphic *RET* allele, resulting from a common noncoding polymorphism (59). On the other hand, no chromosome 21 gene has been formally identified as predisposing to HSCR. Indeed, no gene with a proven role in ENS formation has been shown to reside on chromosome 21q so far. Although *DSCAM* was previously suggested as such a candidate (12, 13), our RNAseq data indicate that this gene was only weakly expressed in eNCCs (Supplemental Data Set 1). Moreover, based on what is known regarding the role of DSCAM in other contexts, only loss-of-function mutations would be compatible with a negative impact, if any, on eNCC migration (60–62). In light of our results with the Holstein mouse line and human patients with HSCR with or without Down syndrome, several lines of evidence now suggest that the *COL6A1-COL6A2* gene pair represents a more solid candidate: (a) it is, like *DSCAM*, included in the approximately 13-Mb region shared by patients with Down syndrome and HSCR (13); (b) it is expressed in several tissues during development (63), including eNCCs (ref. 11 and this work); (c) it is overexpressed in trisomy 21 fetuses (64) and early postnatal bowels (this work); (d) it encodes the two α chains that are instrumental for assembly of all subtypes of collagen VI trimeric monomers (24, 25); and (d) high levels of mature extracellular collagen VI microfilaments are clearly detrimental for eNCC migration (this work). In contrast to what we found with the Holstein line, it is noteworthy that the split and nonfunctional *COL6A4* gene in humans is not expected to contribute to the increased collagen VI deposition observed in HSCR tissues (Figure 7 and Supplemental Figure 11). In these circumstances — and based on our RNAseq data for murine eNCCs, the α1 and α2 chains are thus expected to exclusively interact with the α3 chain and thereby only form "classical" α1-α2-α3 trimeric monomers in human eNCCs.

Conclusion. Our previous analysis of the TashT line showed that, among several pathways and processes affected, the mutant eNCCs were notably found to impose major changes on the composition of their own ECM, including increased collagen VI levels (11). With the Holstein line, we now demonstrate that the single alteration of collagen VI levels in the ECM surrounding eNCCs is enough by itself to cause aganglionosis. This cumulative work suggests that the ECM of the gut wall is a major player in ENS formation. Targeting this previously overlooked aspect of ENS development could have clinical relevance for the cell-based therapies currently being developed for treatment of enteric neuropathies (65).

Methods

Mice. The Holstein transgenic mouse line was generated in the FVB/N background via standard pronuclear injection (66). Two transgenes were coinjected: a *Tyr* minigene to allow visual identification of transgenic animals via rescue of pigmentation (38) and a *SOX3*p-GFP construct. This second transgene was aimed at marking neural and gonadal cells with GFP fluorescence but was not expressed in the Holstein line. To facilitate analyses, the Holstein line was intercrossed with

a previously described mouse line also kept on the FVB/N background in which eNCCs express the DsRed2 fluorescent marker (G4-RFP) (40). For embryo analyses, mice were mated overnight, and noon on the day that a vaginal plug was observed was designated as E0.5. Genotyping of adult Holstein and G4-RFP animals was performed by visual inspection of coat color, whereas genotyping of the Holstein allele in embryonic tissues was performed by PCR (see below).

AChE histochemistry. AChE activity was revealed histochemically in accordance to previously described procedures (67). Briefly, whole colons were dissected from P20 mice, cut longitudinally along the mesentery, and fixed in 4% PFA overnight at 4°C. Muscle layers containing the myenteric plexus were mechanically separated from mucosal/submucosal tissues by microdissection and subsequently incubated in saturated sodium sulfate overnight at 4°C. Preparations were then transferred in a prestaining buffer (0.2 mM ethopropazine HCl, 4 mM acetylthiocholine iodide, 10 mM glycine, 2 mM cupric sulfate, and 65 mM sodium acetate, pH 5.5) for 2 to 4 hours. Staining for AChE was developed by incubation in sodium sulfide for 1.5 minutes (1.25%, pH 6), after which tissues were rinsed extensively with tap water. Images were acquired with a Leica DFC 495 camera mounted on a Leica M205 FA stereomicroscope (Leica Microsystems Canada).

FACS and RNA extraction. Whole intestines were dissected from E12.5 embryos obtained from $Hol^{Tg/+}$ G4-RFP intercrosses and individually dissociated at 37°C in EMEM containing collagenase (0.4 mg/ml; Sigma-Aldrich C2674), dispase II (1.3 mg/ml; Life Technologies 17105-041), and DNAse I (0.5 mg/ml; Sigma-Aldrich DN25). Single RFP-positive viable cells (between 10,000 and 20,000 cells per intestine) were collected from each individual preparation using a MoFlo XDP (Beckman Coulter) cell sorter and frozen at –80°C. Following genotyping by PCR using embryo heads as a DNA source (see below), samples of FACS-recovered cells were processed for RNA extraction either individually (for semiquantitative RT-PCR) or in groups of 5 to 6 (for RNAseq). Total RNA was extracted using the RNeasy Plus Purification Mini Kit in accordance with the manufacturer's instructions (Qiagen).

Genotyping PCR and semiquantitative RT-PCR. Genotyping of the Holstein allele was performed using a standard Taq DNA polymerase (Feldan) and the primers depicted in Figure 3A. Semiquantitative RT-PCR analyses were carried out using 10 ng total RNA with the OneStep RT-PCR Kit (Qiagen) and primers specific to the desired target, using *Gapdh* for normalization. PCR consisted of 35 cycles of 30 seconds at 95°C, 40 seconds at 60°C, and 30 seconds at 72°C. Amplicons were resolved on a 2% agarose gel. Primer details can be found in Supplemental Table 2.

High-throughput genome and transcriptome sequencing. Whole-genome and transcriptome library generation and sequencing (Illumina HiSeq 2000) as well as bioinformatics analyses were performed at the McGill University and Génome Québec Innovation Centre as previously described (11). For RNA sequencing, rRNA-depleted libraries were prepared using 100 ng total RNA per sample, and 3 biological replicates per genotype were analyzed (each containing FACS-recovered eNCCs from 5 to 6 embryos). From 300- to 500-bp library inserts, around 200 million paired-end sequences (100-bp length) were obtained for the $Hol^{Tg/Tg}$ genomic DNA, whereas between 55 and 70 million paired-end sequences were obtained for each of the transcriptome samples. Sequences were mapped onto the mm10 *Mus musculus* reference genome. Results of the differential gene expression analysis were generated using DESeq and edgeR R Bioconductor

packages, with *P* values adjusted using the Benjamini-Hochberg (false discovery rate) procedure.

Heterotopic grafting experiments. Grafting of E12.5 midgut segments (control G4-RFP vs. mutant $Hol^{Tg/Tg}$ G4-RFP) on control hindgut segments (free of eNCCs) were performed as previously described (20). Briefly, each graft was assembled on a small nitrocellulose filter (Millipore GSWP01300), and each graft-attached filter (with graft facing up) was then deposited in a well of 8-chamber slides (ibiTreat μ-slide, Ibidi). The samples were cultured in DMEM/F12 containing 10% FBS and penicillin/streptomycin at 37°C, 5% CO_2. After 24 hours of culture, images were acquired with an Infinity-2 camera (Lumenera Corporation) mounted on a Leica M205FA stereomicroscope. Colonization of hindgut tissues by midgut-derived eNCCs was then quantified using ImageJ software by measuring the distance separating the most distal fluorescently labeled eNCC from the midgut-hindgut graft junction.

Ex vivo time-lapse imaging of eNCCs. Live imaging of eNCCs was performed using a previously described suspended culture technique (68). Briefly, E12.5 and E13.5 whole-embryonic intestines were placed on a small nitrocellulose filter (Millipore GSWP01300). The gut-attached filter paper was suspended, with the tissue side on paraffin bridges streaked in parallel on a 60-mm cell culture dish (Corning). The samples were cultured in DMEM/F12 containing 10% FBS and penicillin/streptomycin at 37°C, 5% CO_2, over 10 hours in a microscope incubation chamber (Okolab). Image stacks (250-μm thick) were acquired every 10 minutes using a ×10 objective and a Nikon A1R confocal unit. For calculations of speed and directionality, 6 to 7 chain tip cells were tracked from at least 3 intestines of each genotype as previously described (11). The trajectories were determined by drawing a straight line relative to the longitudinal axis of the gut from the cell position at 0 hours and the radial position (in degrees) of the same cell at 10 hours.

Ex vivo migration assays. Cultures of embryonic intestinal explants were adapted from previously described procedures (69). Briefly, manually cut transverse sections (~500 μm) of E12.5 small bowel (control G4-RFP or $Hol^{Tg/Tg}$ G4-RFP) were cultured in 8-chamber slides (ibiTreat μ-slide, Ibidi) precoated with fibronectin (Millipore FC010), gelatin (Sigma-Aldrich G1890), collagen I (Corning 354236), or collagen VI (Corning 354261). Coatings were prepared by depositing 500 μl of 250 μg/ml solution in each well and incubating for 30 minutes, followed by 2 washes in PBS. For fibronectin/collagen VI competition experiments, coatings were prepared with solutions containing 250 μg/ml fibronectin and increasing amounts of collagen VI (1:0.5 and 1:1 concentration ratios). Explants were cultured in serum-free DMEM/F12 medium (containing penicillin/streptomycin and 1% N2 supplement [Invitrogen]) supplemented with 50 ng/ml GDNF (Cedarlane CLCYT305-2). Cultures were maintained for 48 hours (37°C, 5% CO_2), after which time images were acquired with a ×4 objective and a Nikon A1 epifluorescence microscope. Cell migration was assessed using ImageJ software by measuring the distance separating the most distal fluorescently labeled eNCC from the edge of the explant in 8 equivalent quadrants around the explant.

Human colon tissues. All HSCR tissue specimens were obtained from the "healthy" ganglionated zone (corresponding to the sigmoid colon) — as confirmed by histopathological analysis — following rectosigmoid resection via a transanal Soave pull-through. Patients in the HSCR case group (*n* = 12; 10 boys and 2 girls; aged between 17 and 454 days at the time of surgery) had only short-segment HSCR

(i.e., without Down syndrome or other congenital malformations). Patients in the Down syndrome HSCR case group (n = 4; 3 boys and 1 girl; aged between 49 and 334 days at the time of surgery) had Down syndrome and short-segment HSCR. Samples from the control group (n = 8; 7 boys and 1 girl; aged between 1 and 452 days at the time of surgery) were obtained from patients with anorectal malformation (7 patients from whom tissues were collected at the time of initial surgery or sigmoidostomy closure) or with long-gap esophageal atresia (patient C3 who underwent colonic interposition using transverse and left colon). All colonic tissues were devoid of overt signs of inflammation at the time of tissue collection and were processed for sectioning (15-μm transverse sections) by the Histology platform of the Institut de Recherche en Immunologie et Cancer (Montreal, Canada). Details regarding each analyzed tissue can be found in Supplemental Table 1.

Immunofluorescence staining. Whole-mouse embryonic intestines and transverse sections of human colonic tissues (pretreated for antigen retrieval via boiling in a solution of sodium citrate, pH 6.0, for 10 minutes) were permeabilized for 2 hours with PBS/FBS (10%)/Triton X-100 (0.1%). Tissues were then sequentially incubated with specific primary (at 4°C overnight) and relevant secondary antibodies (at room temperature for 3 hours) diluted 1:500 in the same buffer. All antibodies used in this study are listed in Supplemental Table 3. TUNEL assays were performed using the TMR Red In Situ Cell Death Detection Kit in accordance with the manufacturer's instructions (Roche Applied Science). Images were acquired with either a ×20 or a ×60 objective on a Nikon A1R confocal unit. To quantify immunofluorescence signal, relevant images were taken with the exact same acquisition settings. Fluorescence intensity within a defined field was assessed using ImageJ software and expressed in candela/μm². This defined field was of fixed dimension (100 μm × 100 μm) for mouse embryonic tissues or corresponded to a 10-μm-wide strip around each myenteric ganglion for human postnatal tissues. For quantitative analyses of cell differentiation, the number of HuC/D⁺, S100β⁺, and SOX10⁺ cells was counted in at least 3 microscopic fields per intestine and expressed as a percentage of the total number of eNCCs (HuC/D⁺ cells plus SOX10⁺ cells).

Statistics. Where applicable, data are expressed as the mean ± SEM, with the number of independent biological replicates (n) indicated in the figure and/or legend. The significance of differences was determined through 1-way ANOVA (when 3 groups were involved) or 2-tailed Student's t test (when 2 groups were involved) using GraphPad software. Differences were considered statistically significant at $P < 0.05$.

Study approval. Experiments with mice were carried out in accordance with the guidelines of the Canadian Council on Animal Care and approved by the relevant institutional committee (Comité institutionnel de protection des animaux, reference 650) of UQAM. Human samples were collected after obtaining informed consent on behalf of the children involved (from either the parents or legal guardians). This multicenter study (University Hospitals of Nantes,

Poitiers, Brest, and Angers, France; Necker Hospital, Paris, France; and Sainte-Justine University Health Center, Montreal, Canada) was approved by the Groupe Nantais d'Éthique dans le Domaine de la Santé (Nantes, France) under protocol 16-12-2014 as well as by the Comité d'éthique de la recherche of the Sainte-Justine University Health Centre (Montreal, Canada) under protocol 4172. Biocollection performed by the Ente-Hirsch study group related to this study was approved by the Comité de Protection des Personnes Ouest IV (Nantes, France) and was declared to the Ministry of Research and Higher Education. The database of the biocollection is in compliance with the requirements of the French data protection authority (Commission Nationale Informatique et Libertés).

Author contributions

Acknowledgments

Address correspondence to: Nicolas Pilon, Department of Biological Sciences and BioMed Research Center, Faculty of Sciences, University of Quebec at Montreal (UQAM), 141 President-Kennedy Ave., Montreal, Quebec, Canada, H2X 3Y7. Phone: 514.987.3000, ext. 3342; E-mail: pilon.nicolas@uqam.ca.

1. Furness JB. The enteric nervous system and neurogastroenterology. *Nat Rev Gastroenterol Hepatol.* 2012;9(5):286–294.
2. Anderson RB, Newgreen DF, Young HM. Neural crest and the development of the enteric nervous system. *Adv Exp Med Biol.* 2006;589:181–196.
3. Heanue TA, Pachnis V. Enteric nervous system development and Hirschsprung's disease:

advances in genetic and stem cell studies. *Nat Rev Neurosci.* 2007;8(6):466–479.
4. Obermayr F, Hotta R, Enomoto H, Young HM. Development and developmental disorders of the enteric nervous system. *Nat Rev Gastroenterol Hepatol.* 2013;10(1):43–57.
5. Bergeron KF, Silversides DW, Pilon N. The developmental genetics of Hirschsprung's disease.

Clin Genet. 2013;83(1):15–22.
6. Goldstein AM, Hofstra RM, Burns AJ. Building a brain in the gut: development of the enteric nervous system. *Clin Genet.* 2013;83(4):307–316.
7. Lake JI, Heuckeroth RO. Enteric nervous system development: migration, differentiation, and disease. *Am J Physiol Gastrointest Liver Physiol.* 2013;305(1):G1–G24.

8. Amiel J, et al. Hirschsprung disease, associated syndromes and genetics: a review. *J Med Genet*. 2008;45(1):1–14.

9. Barlow A, de Graaff E, Pachnis V. Enteric nervous system progenitors are coordinately controlled by the G protein-coupled receptor EDNRB and the receptor tyrosine kinase RET. *Neuron*. 2003;40(5):905–916.

10. Alves MM, et al. Contribution of rare and common variants determine complex diseases-Hirschsprung disease as a model. *Dev Biol*. 2013;382(1):320–329.

11. Bergeron KF, et al. Male-biased aganglionic megacolon in the TashT mouse line due to perturbation of silencer elements in a large gene desert of chromosome 10. *PLoS Genet*. 2015;11(3):e1005093.

12. Jannot AS, et al. Chromosome 21 scan in Down syndrome reveals DSCAM as a predisposing locus in Hirschsprung disease. *PLoS One*. 2013;8(5):e62519.

13. Korbel JO, et al. The genetic architecture of Down syndrome phenotypes revealed by high-resolution analysis of human segmental trisomies. *Proc Natl Acad Sci U S A*. 2009;106(29):12031–12036.

14. Li Y, Kido T, Garcia-Barcelo MM, Tam PK, Tabatabai ZL, Lau YF. SRY interference of normal regulation of the RET gene suggests a potential role of the Y-chromosome gene in sexual dimorphism in Hirschsprung disease. *Hum Mol Genet*. 2015;24(3):685–697.

15. Wallace AS, Tan MX, Schachner M, Anderson RB. L1cam acts as a modifier gene for members of the endothelin signalling pathway during enteric nervous system development. *Neurogastroenterol Motil*. 2011;23(11):e510–e522.

16. Hynes RO, Naba A. Overview of the matrisome — an inventory of extracellular matrix constituents and functions. *Cold Spring Harb Perspect Biol*. 2012;4(1):a004903.

17. Bonnans C, Chou J, Werb Z. Remodelling the extracellular matrix in development and disease. *Nat Rev Mol Cell Biol*. 2014;15(12):786–801.

18. Mouw JK, Ou G, Weaver VM. Extracellular matrix assembly: a multiscale deconstruction. *Nat Rev Mol Cell Biol*. 2014;15(12):771–785.

19. Breau MA, Dahmani A, Broders-Bondon F, Thiery JP, Dufour S. Beta1 integrins are required for the invasion of the caecum and proximal hindgut by enteric neural crest cells. *Development*. 2009;136(16):2791–2801.

20. Breau MA, et al. Lack of beta1 integrins in enteric neural crest cells leads to a Hirschsprung-like phenotype. *Development*. 2006;133(9):1725–1734.

21. Akbareian SE, et al. Enteric neural crest-derived cells promote their migration by modifying their microenvironment through tenascin-C production. *Dev Biol*. 2013;382(2):446–456.

22. Barriga EH, Trainor PA, Bronner M, Mayor R. Animal models for studying neural crest development: is the mouse different? *Development*. 2015;142(9):1555–1560.

23. Knupp C, Squire JM. A new twist in the collagen story — the type VI segmented supercoil. *EMBO J*. 2001;20(3):372–376.

24. Fitzgerald J, Holden P, Hansen U. The expanded collagen VI family: new chains and new questions. *Connect Tissue Res*. 2013;54(6):345–350.

25. Gara SK, et al. Three novel collagen VI chains with high homology to the alpha3 chain. *J Biol Chem*. 2008;283(16):10658–10670.

26. Fitzgerald J, Rich C, Zhou FH, Hansen U. Three novel collagen VI chains, α4(VI), α5(VI), and α6(VI). *J Biol Chem*. 2008;283(29):20170–20180.

27. Gara SK, et al. Differential and restricted expression of novel collagen VI chains in mouse. *Matrix Biol*. 2011;30(4):248–257.

28. Bonaldo P, Braghetta P, Zanetti M, Piccolo S, Volpin D, Bressan GM. Collagen VI deficiency induces early onset myopathy in the mouse: an animal model for Bethlem myopathy. *Hum Mol Genet*. 1998;7(13):2135–2140.

29. Bonnemann CG. The collagen VI-related myopathies: muscle meets its matrix. *Nat Rev Neurol*. 2011;7(7):379–390.

30. Dassah M, Almeida D, Hahn R, Bonaldo P, Worgall S, Hajjar KA. Annexin A2 mediates secretion of collagen VI, pulmonary elasticity and apoptosis of bronchial epithelial cells. *J Cell Sci*. 2014;127(pt 4):828–844.

31. Pan TC, et al. A mouse model for dominant collagen VI disorders: heterozygous deletion of Col6a3 Exon 16. *J Biol Chem*. 2014;289(15):10293–10307.

32. Pan TC, et al. COL6A3 protein deficiency in mice leads to muscle and tendon defects similar to human collagen VI congenital muscular dystrophy. *J Biol Chem*. 2013;288(20):14320–14331.

33. Groulx JF, Gagne D, Benoit YD, Martel D, Basora N, Beaulieu JF. Collagen VI is a basement membrane component that regulates epithelial cell-fibronectin interactions. *Matrix Biol*. 2011;30(3):195–206.

34. Perris R, Kuo HJ, Glanville RW, Bronner-Fraser M. Collagen type VI in neural crest development: distribution in situ and interaction with cells ex vivo. *Dev Dyn*. 1993;198(2):135–149.

35. Sabatelli P, et al. Collagen VI deficiency affects the organization of fibronectin in the extracellular matrix of cultured fibroblasts. *Matrix Biol*. 2001;20(7):475–486.

36. Kuo HJ, Maslen CL, Keene DR, Glanville RW. Type VI collagen anchors endothelial basement membranes by interacting with type IV collagen. *J Biol Chem*. 1997;272(42):26522–26529.

37. Tillet E, et al. Recombinant expression and structural and binding properties of α1(VI) and α2(VI) chains of human collagen type VI. *Eur J Biochem*. 1994;221(1):177–185.

38. Methot D, Reudelhuber TL, Silversides DW. Evaluation of tyrosinase minigene co-injection as a marker for genetic manipulations in transgenic mice. *Nucleic Acids Res*. 1995;23(22):4551–4556.

39. Moore SW, Johnson G. Acetylcholinesterase in Hirschsprung's disease. *Pediatric surgery international*. 2005;21(4):255–263.

40. Pilon N, Raiwet D, Viger RS, Silversides DW. Novel pre- and post-gastrulation expression of Gata4 within cells of the inner cell mass and migratory neural crest cells. *Dev Dyn*. 2008;237(4):1133–1143.

41. Mwizerwa O, Das P, Nagy N, Akbareian SE, Mably JD, Goldstein AM. Gdnf is mitogenic, neurotrophic, and chemoattractive to enteric neural crest cells in the embryonic colon. *Dev Dyn*. 2011;240(6):1402–1411.

42. Young HM, Hearn CJ, Farlie PG, Canty AJ, Thomas PQ, Newgreen DF. GDNF is a chemoattractant for enteric neural cells. *Dev Biol*. 2001;229(2):503–516.

43. Newgreen DF, Hartley L. Extracellular matrix and adhesive molecules in the early development of the gut and its innervation in normal and spotting lethal rat embryos. *Acta Anat (Basel)*. 1995;154(4):243–260.

44. Edery P, et al. Mutations of the RET proto-oncogene in Hirschsprung's disease. *Nature*. 1994;367(6461):378–380.

45. Romeo G, et al. Point mutations affecting the tyrosine kinase domain of the RET proto-oncogene in Hirschsprung's disease. *Nature*. 1994;367(6461):377–378.

46. Jiang Q, et al. Functional loss of semaphorin 3C and/or semaphorin 3D and their epistatic interaction with ret are critical to Hirschsprung disease liability. *Am J Hum Genet*. 2015;96(4):581–596.

47. Fernandez RM, et al. Pathways systematically associated to Hirschsprung's disease. *Orphanet J Rare Dis*. 2013;8:187.

48. Tang CS, et al. Genome-wide copy number analysis uncovers a new HSCR gene: NRG3. *PLoS Genet*. 2012;8(5):e1002687.

49. Dixon JR, et al. Topological domains in mammalian genomes identified by analysis of chromatin interactions. *Nature*. 2012;485(7398):376–380.

50. Narendra V, et al. Transcription. CTCF establishes discrete functional chromatin domains at the Hox clusters during differentiation. *Science*. 2015;347(6225):1017–1021.

51. Nora EP, et al. Spatial partitioning of the regulatory landscape of the X-inactivation centre. *Nature*. 2012;485(7398):381–385.

52. Lupianez DG, et al. Disruptions of topological chromatin domains cause pathogenic rewiring of gene-enhancer interactions. *Cell*. 2015;161(5):1012–1025.

53. Lupski JR. Genomic rearrangements and sporadic disease. *Nat Genet*. 2007;39(7 suppl):S43–S47.

54. Stankiewicz P, Lupski JR. Structural variation in the human genome and its role in disease. *Annu Rev Med*. 2010;61:437–455.

55. Fujimoto T, Hata J, Yokoyama S, Mitomi T. A study of the extracellular matrix protein as the migration pathway of neural crest cells in the gut: analysis in human embryos with special reference to the pathogenesis of Hirschsprung's disease. *J Pediatr Surg*. 1989;24(6):550–556.

56. Rozario T, DeSimone DW. The extracellular matrix in development and morphogenesis: a dynamic view. *Dev Biol*. 2010;341(1):126–140.

57. De Bellard ME, Rao Y, Bronner-Fraser M. Dual function of Slit2 in repulsion and enhanced migration of trunk, but not vagal, neural crest cells. *J Cell Biol*. 2003;162(2):269–279.

58. Delabar JM, et al. Molecular mapping of twenty-four features of Down syndrome on chromosome 21. *Eur J Hum Genet*. 1993;1(2):114–124.

59. Arnold S, et al. Interaction between a chromosome 10 RET enhancer and chromosome 21 in the Down syndrome-Hirschsprung disease association. *Hum Mutat*. 2009;30(5):771–775.

60. Fusaoka E, Inoue T, Mineta K, Agata K, Takeuchi K. Structure and function of primitive immunoglobulin superfamily neural cell adhesion mole-

cules: a lesson from studies on planarian. *Genes Cells*. 2006;11(5):541–555.

61. Liu G, et al. DSCAM functions as a netrin receptor in commissural axon pathfinding. *Proc Natl Acad Sci U S A*. 2009;106(8):2951–2956.

62. Ly A, Nikolaev A, Suresh G, Zheng Y, Tessier-Lavigne M, Stein E. DSCAM is a netrin receptor that collaborates with DCC in mediating turning responses to netrin-1. *Cell*. 2008;133(7):1241–1254.

63. Gitton Y, et al. A gene expression map of human chromosome 21 orthologues in the mouse.

Nature. 2002;420(6915):586–590.

64. von Kaisenberg CS, Brand-Saberi B, Christ B, Vallian S, Farzaneh F, Nicolaides KH. Collagen type VI gene expression in the skin of trisomy 21 fetuses. *Obstet Gynecol*. 1998;91(3):319–323.

65. Burns AJ, Thapar N. Neural stem cell therapies for enteric nervous system disorders. *Nat Rev Gastroenterol Hepatol*. 2014;11(5):317–328.

66. Nagy A, Gertsenstein M, Vintersten K, Behringer R. *Manipulating The Mouse Embryo, A Laboratory Manual*. 3rd ed. Cold Spring Harbor, New York, New York, USA: Cold Spring Harbor Laboratory

Press; 2003.

67. Enomoto H, et al. GFR α1-deficient mice have deficits in the enteric nervous system and kidneys. *Neuron*. 1998;21(2):317–324.

68. Nishiyama C, et al. Trans-mesenteric neural crest cells are the principal source of the colonic enteric nervous system. *Nat Neurosci*. 2012;15(9):1211–1218.

69. Lake JI, Tusheva OA, Graham BL, Heuckeroth RO. Hirschsprung-like disease is exacerbated by reduced de novo GMP synthesis. *J Clin Invest*. 2013;123(11):4875–4887.